# Electron Spin Resonance of Ti$^{3+}$
# in Synthetic Beryl

*D. R. Hutton, J. R. Pilbrow, G. J. Troup and J. O. Warne*

Department of Physics, Monash University,
Clayton, Vic. 3168, Australia.

*Abstract*

Synthetic Australian Biron beryl, coloured pink by titanium, shows an ESR spectrum due to Ti$^{3+}$ substituted into the trigonally distorted Al$^{3+}$ octahedral site of the crystal structure. The ESR spectrum can be fitted with an axial spin Hamiltonian

$$\mathcal{H} = \beta \boldsymbol{B}.\mathbf{g}.\boldsymbol{S} + \boldsymbol{I}.\mathbf{A}.\boldsymbol{S},$$

with parameters

$$g_{||} = 1 \cdot 987 \pm 0 \cdot 001, \qquad g_{\perp} = 1 \cdot 842 \pm 0 \cdot 001,$$

$$A_{||} = (0 \cdot 0 \pm 0 \cdot 1) \times 10^{-4} \text{ cm}^{-1}, \qquad A_{\perp} = (18 \cdot 0 \pm 0 \cdot 1) \times 10^{-4} \text{ cm}^{-1}.$$

Lines are broad at room temperature (linewidth of 6 mT) but narrow sufficiently ($1 \cdot 2$ mT) at $-120°$C to resolve the hyperfine structure, and allow the detection of nearest neighbour axial pairs with $D = 0 \cdot 028$ cm$^{-1}$.

## 1. Introduction

Beryl is an important ring silicate mineral, both to the gem industry and increasingly to the laser industry. It occurs in nature in large crystals with a broad range of colours including green (emerald), blue (aquamarine), yellow (heliodor), red (bixbite) and pink (morganite). It may also be synthesised relatively easily by the flux melt method (Chatham, Gilson) or the hydrothermal method (Linde, Biron).

The colour of beryl may be caused by irradiation (e.g. blue Maxixe), but more often is due to the substitution of transition metal impurities in either the Be$^{2+}$ tetrahedral sites, or the two inversion related Al$^{3+}$ octahedral sites which bind the Si$_6$O$_{18}$ rings together (Deer *et al.* 1986). Ions and molecules may also be accommodated in the open ring channels, and these may themselves be chromophoric or charge compensate other valence ions in the substitutional sites.

In a recent report (Hutton *et al.* 1991) we described the ESR detection of vanadium in high quality green synthetic beryl grown by Biron International, Perth, Australia. The present study reports the results on equally high quality pink beryl, which is produced without the normally associated impurity manganese as colouring agent. Once again ESR gives a very useful probe of the transition metal impurity sites, both single ions and pairs, and a good measure of the crystal

quality. $Ti^{3+}$ complexes have been studied relatively little by ESR (Abragam and Bleaney 1970) because many of them are unstable, but also because many have large linewidths at higher temperatures. Consequently their detection in natural materials is quite rare.

## 2. ESR Experimental

A small high quality pale pink synthetic crystal was supplied by Biron International, Perth. This contains a 1% fraction of $Ti^{3+}$ together with a trace of $Cr^{3+}$ remaining from the feedstock beryl material supplied during the hydrothermal growth. ESR experiments were carried out using X-band spectrometers (Varian E12 and a purpose built single crystal spectrometer) at temperatures from $+40°C$ to $-160°C$. The highly anisotropic spectrum of $Cr^{3+}$ (Geusic *et al.* 1959) together with the sharp $Cr^{3+}$ line allowed accurate alignments of the crystal in the microwave cavity. So perfect was the crystal supplied that the $^{53}Cr^{3+}$ hyperfine structure from this 10% abundant isotope could be easily determined ($A_{\parallel} = 1.75$ mT, linewidth $0.15$ mT).
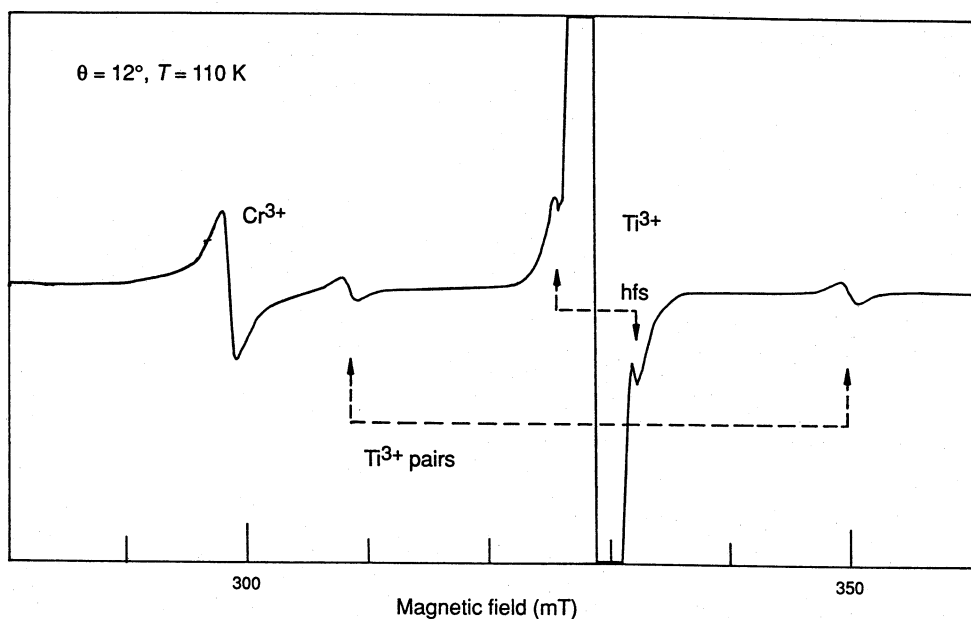


**Fig. 1.** ESR spectrum at 110 K, 12° from the *c*-axis showing $Cr^{3+}$ and $Ti^{3+}$ hyperfine structure (hfs) and $Ti^{3+}$ pair lines.

At room temperature the relatively weak simple $g \sim 2$ line was $\sim 6$ mT wide and no hyperfine structure was observable. However, at 110 K the line had narrowed to $\sim 1.2$ mT, increased its signal height by a factor of $\sim 70$, and the $^{47}Ti$ and $^{49}Ti$ hyperfine structure was well-resolved. In addition, two pair lines 44 mT (440 G) apart were observable on the *c*-axis, and 25 mT (250 G) apart perpendicular to the *c*-axis, just outside the range of the hyperfine lines. They appear to fit a $(3\cos^2\theta - 1)$ angular dependence expected for $S = 1$ and the transitions cross when $\theta = 53.5°$. Fig. 1 illustrates the spectra observed. A study of the spectral

line positions as the magnetic field direction is varied relative to the crystal demonstrated that the Zeeman, hyperfine and pair interactions were all axial, and hence almost certainly arose from Ti$^{3+}$ ions in trigonal Al$^{3+}$ sites, and the nearest neighbour axial pairs respectively. The crystal was carefully rotated from the c-axis and spectra were accumulated in computer storage for simulation and fitting.

**Table 1. Nuclear and hyperfine data for titanium isotopes**

| Isotope | $I$ | Abundance (%) | $\mu/\mu_n$ | $g_n$ | Hyperfine structure |
|---|---|---|---|---|---|
| *Even* | | | | | |
| $^{46}$Ti | 0 | 8 | | | No |
| $^{48}$Ti | 0 | 74 | | | No |
| $^{50}$Ti | 0 | 5 | | | No |
| *Odd* | | | | | |
| $^{47}$Ti | $\frac{5}{2}$ | 7·3 | −0·79 | 2·758 | Yes |
| $^{49}$Ti | $\frac{7}{2}$ | 5·5 | −1·10 | 2·760 | Yes |
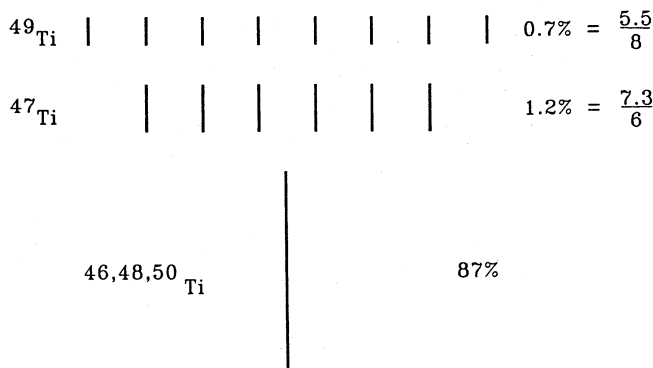


**Fig. 2.** Expected form of the Ti$^{3+}$ ESR spectrum.

## 3. Interpretation of ESR

### (a) Isolated Titanium Ion Spectra—Spin Hamiltonian

The expected ESR spectrum should be characterised by a strong central line from the even isotopes (total abundance 87%) and overlapping sets of six hyperfine lines from $^{47}$Ti and eight lines from $^{49}$Ti. As can be seen from Table 1, the nuclear moments for both $^{47}$Ti and $^{49}$Ti are almost identical. This means that all but the outer lines from $^{49}$Ti will be superimposed on the $^{47}$Ti lines. Therefore, one expects the spectrum to consist of the line due to the even isotopes with relative intensity 87% at the centre of the satellite hyperfine structure, consisting of eight lines with intensities 0·7:1·9:1·9:1·9:1·9:1·9:1·9:0·7% (see Fig. 2). The spin Hamiltonian appropriate for Ti$^{3+}$(3d$^1$) is given by

$$\mathcal{H} = \beta[g_{\parallel} B_z S_z + g_{\perp}(B_x S_x + B_y S_y)] + A_{\parallel} S_z I_z + A_{\perp}(S_x I_x + S_y I_y), \quad (1)$$

where $S = \frac{1}{2}$ and $I = 0$ for the even isotopes of titanium and $I = \frac{5}{2}$ and $\frac{7}{2}$ respectively for $^{47}$Ti and $^{49}$Ti. As already mentioned, the near equivalence of the nuclear moments for the latter two isotopes means that the hyperfine constants will be identical, even though they have different numbers of hyperfine lines.

The angular variation of **g** is given by the familiar formula

$$g^2 = g_{||}^2 \cos^2\theta + g_\perp^2 \sin^2\theta , \tag{2}$$

which is exact for a true $S = \frac{1}{2}$ system. The well-known expression for angular variation for the hyperfine structure is
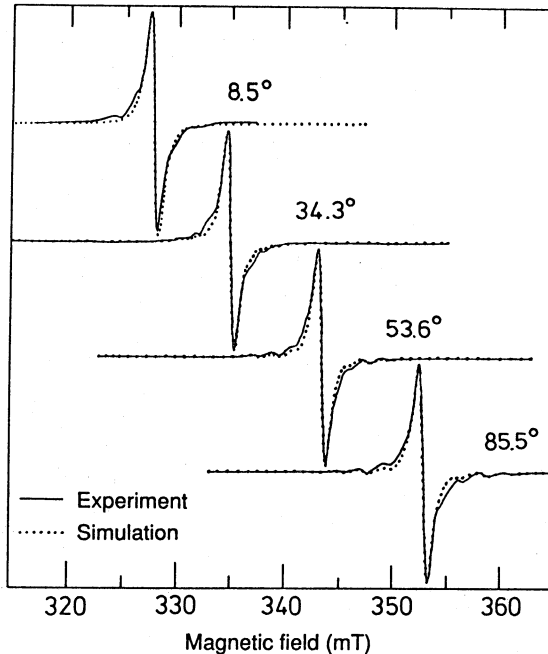
$$A^2 g^2 = A_{||}^2 g_{||}^2 \cos^2\theta + A_\perp^2 g_\perp^2 \sin^2\theta , \tag{3}$$

but this is a result correct only to first order in perturbation theory. The resonance fields for the transitions are given by

$$B = B_0 - \frac{A}{g\beta} + ... , \tag{4}$$

Table 2. **Spin Hamiltonian parameters for Ti$^{3+}$ in beryl**

|  | g factor | A values ($10^{-4}$ cm$^{-1}$) | Linewidth (mT) |
|---|---|---|---|
| \|\| | $1\cdot987\pm0\cdot001$ | $0\cdot0\pm0\cdot1$ | $0\cdot7$ |
| $\perp$ | $1\cdot842\pm0\cdot001$ | $18\cdot0\pm0\cdot1$ | $0\cdot75$ |



Fig. 3. Experimental and simulated ESR spectrum for Ti$^{3+}$ in beryl.

where $B_0 = h\nu/g\beta$. We do not need to consider the higher order terms in equation (4) since the analysis was based on an exact diagonalisation of the spin Hamiltonian and the inherent limitations of perturbation approximations were avoided. Clearly the resonance field for the even isotopes of titanium could be obtained exactly from equation (4) by putting $A = 0$.

The diagonalisation was carried out for a number of experimental orientations, i.e. values of $\theta$, the value of the magnetic field being iterated until the energy differences (between the eigenvalues) equalled the microwave energy $h\nu$. The field at which equality was achieved was the resonance field used in the simulations. Since we are dealing here with single crystals, and only one site, the simulation consisted of nine transitions as described above with relative intensities determined by the natural isotropic abundances given in Table 1. The lineshape turned out to be more Lorentzian in shape than Gaussian and the first derivatives were obtained as shown in Fig. 3. The spin Hamiltonian parameters are given in Table 2.

As can be seen the lineshapes do not fit exactly, reflecting the fact that they are quite complicated. For examples of lineshapes due to different mechanisms operating in solids, see the review by Stoneham (1969) and the book by one of the authors (Pilbrow 1990).
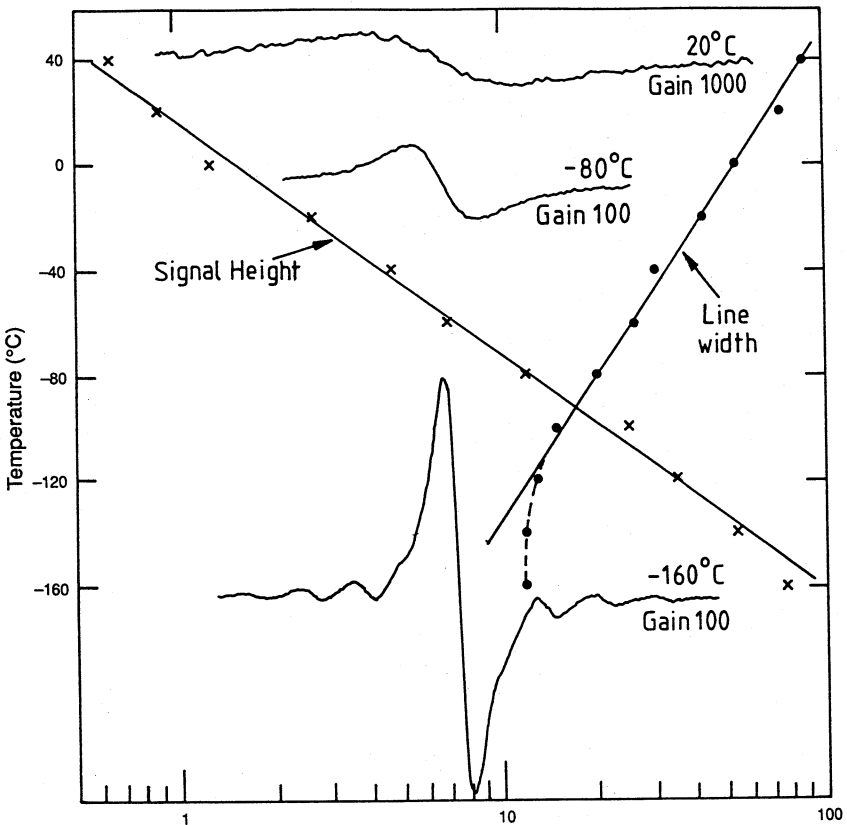


**Fig. 4.** Temperature variation of linewidth and signal height for Ti$^{3+}$ in beryl, for $\theta = 90°$.

*(b) Titanium Pairs*

These pairs can be described by the spin Hamiltonian

$$\mathcal{H} = D(3S_{1z}S_{2z} - \boldsymbol{S}_1 . \boldsymbol{S}_2).\tag{5}$$

The value of $D$ from the experimental data is approximately $0 \cdot 0272\,\mathrm{cm}^{-1}$, determined from a parallel separation between the two lines of $44\,\mathrm{mT}$, and $0 \cdot 0287\,\mathrm{cm}^{-1}$, determined from a perpendicular separation of $25\,\mathrm{mT}$ which, in a first order theory, should be half that in the parallel spectrum. Clearly, second order effects must play some role but this is a little surprising since the lines cross at very nearly the 'magic' angle of $\theta = 54 \cdot 3°$. This matter is not pursued here as it depends on the concentration of $Ti^{3+}$ ions in the lattice. The observation lends further support, on symmetry grounds, to the conclusion that $Ti^{3+}$ occupies substitutional $Al^{3+}$ sites in the crystals.

*(c) Linewidth*

At room temperatures the ESR line was weak and broad, but lowering the temperature produced significant narrowing and strengthening of the lines as illustrated in Fig. 4. Over the range $40°C$ to $-120°C$, lowering the temperature by $27°C$ decreases the linewidth by a factor of $\sqrt{2}$ and doubles the signal height. Such a logarithmic variation in the spin lattice relaxation time suggests an Orbach process of relaxation via a real intermediate state.

Table 3.   Spin–orbit and trigonal field matrix for $t_{2g}$

| Basis state | $\lvert e_+,+\rangle$ | $\lvert 0,-\rangle$ | $\lvert e_-,-\rangle$ | $\lvert 0,+\rangle$ | $\lvert e_+,-\rangle$ | $\lvert e_-,+\rangle$ |
|---|---|---|---|---|---|---|
| $\langle e_+,+\rvert$ | $\delta+\zeta/2$, | $-\zeta/\sqrt{2}$ | | | | |
| $\langle 0,-\rvert$ | $-\zeta/\sqrt{2}$ | $0$ | | | | |
| $\langle e_-,-\rvert$ | | | $\delta+\zeta/2$ | $-\zeta/\sqrt{2}$ | | |
| $\langle 0,+\rvert$ | | | $-\zeta/\sqrt{2}$ | $0$ | | |
| $\langle e_+,-\rvert$ | | | | | $\delta-\zeta/2$ | |
| $\langle e_-,+\rvert$ | | | | | | $\delta-\zeta/2$ |

## 4. Theory for $Ti^{3+}(3d^1)$ in Trigonal Symmetry

A simple crystal field model provides a sensible place to begin the theoretical analysis. To a good first approximation, one need consider only the $t_{2g}$ orbitals and splittings in octahedral and trigonal fields (see Fig. 5). Suitable orbital basis states are

$$\lvert e_\pm\rangle = \sqrt{\tfrac{2}{3}}\,\lvert \pm 2\rangle - \sqrt{\tfrac{1}{3}}\,\lvert \mp 1\rangle, \qquad \lvert 0\rangle = \lvert 0\rangle.\tag{6}$$

When spin is included there is a total of six states and the $6\times 6$ energy matrix (see Table 3) including the ligand field splittings and spin–orbit coupling can be readily solved as two $2\times 2$ and two $1\times 1$ matrices. Mixing due to spin–orbit coupling modifies the states and leads to linear combinations of $\lvert e_+,+\rangle$ and $\lvert 0,-\rangle$ and also of $\lvert e_-,-\rangle$ and $\lvert 0,+\rangle$, where $+$ and $-$ refer to spin up or down. This matrix has a particularly simple solution since the $2\times 2$ matrices are identical and their eigenvalues are

$$E_\pm/\delta = \tfrac{1}{2}[\eta + \tfrac{1}{2} \pm (\eta^2 + \tfrac{1}{2} \pm \tfrac{9}{4})^{\frac{1}{2}}].\tag{7}$$

Since $\zeta > 0$ and if $\delta > 0$ then the ground state is $E_-$ with corresponding eigenvectors

$$|\psi, +\rangle = a|e_+, +\rangle - b|0, -\rangle, \qquad |\psi, -\rangle = a|e_-, -\rangle - b|0, +\rangle, \qquad (8)$$

where $\eta = \zeta/\delta$ and

$$\frac{a}{b} = -\frac{\sqrt{2}}{\eta + \frac{1}{2} - (\eta^2 + \eta + \frac{9}{4})^{\frac{1}{2}}}. \qquad (9)$$
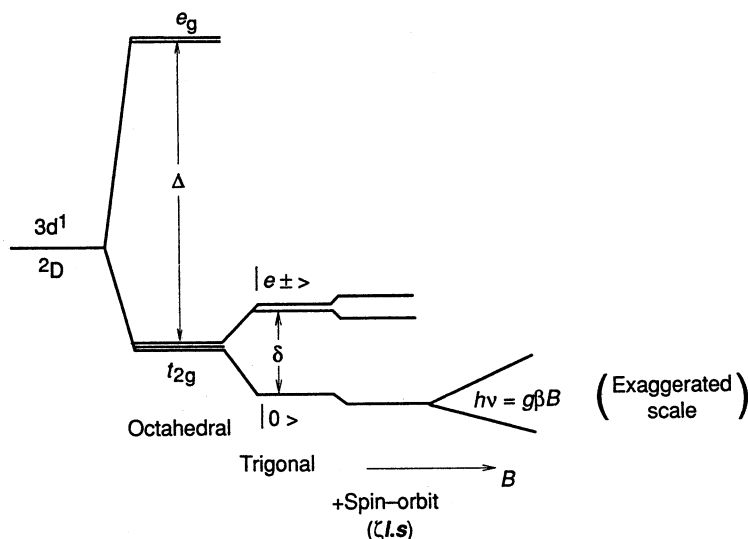


**Fig. 5.** Ground energy levels for $d^1$ in a trigonally distorted octahedral crystal field together with spin–orbit and Zeeman interactions.

While one can pursue the calculation of axial $g$ factors and $A$ values from first principles, they may also be obtained from the theory due to Bleaney and O'Brien (1956) for low spin $d^5$, reversing the sign of $\alpha$ in their theory and putting $a = \sin\alpha$ and $b = \sin\alpha$. These are

$$g_{||} = 2(a^2 - b^2) - 2kb^2, \qquad g_\perp = 2a^2 - 2k\sqrt{2}\,ab, \qquad (10)$$

and

$$A_{||} = 2\mathcal{P}\left(\tfrac{2}{7}a^2 - \tfrac{6}{7}b^2 + \frac{2ab}{7\sqrt{2}} + \frac{k}{2}(b^2 - a^2)\right),$$

$$A_\perp = 2\mathcal{P}\left(\tfrac{1}{7} + \frac{15}{7\sqrt{2}}\,ab + \frac{k}{2}a^2\right), \qquad (11)$$

where

$$\mathcal{P} = \frac{g_e\beta g_n\,\beta_n}{\langle r^{-3}\rangle_{3d}}. \qquad (12)$$

Here $g_e$ is the free electron $g$ factor ($=2\cdot0023$), $\beta$ is the Bohr magneton, $g_n$ is the nuclear $g$ factor for both $^{47}$Ti and $^{49}$Ti since they are very nearly identical, and $\beta_n$ is the nuclear magneton.

What we have to try to explain from Table 2 are the $g$ factors and, what is more critical, the near zero value for $A_\parallel$ and the very small value for $A_\perp$. Clearly for $a \approx 1$, $b \approx 0$ and $k \approx 1$ we have $g_\parallel \approx 2$, $A_\parallel \approx 0$ and $A_\perp \approx \mathcal{P}$, the latter being far too high. A more detailed analysis of the $g$ factors with $k = 1$ gives acceptable agreement with $a$ in the range $0\cdot99855$–$0\cdot99892$ and $b$ in the range $0\cdot05383$–$0\cdot04646$, leading to $g_\parallel$ in the range $1\cdot987$–$1\cdot983$ and $g_\perp$ in the range $1\cdot864$–$1\cdot842$. It is possible to consider $a \approx 1$ and then to attribute $g$ deviations from 2 as being due to excited state interactions via the ligand field. A further deficiency of the present theory is that it does not implicitly include covalency. But since we are dealing with oxygen coordination, this does not seem to be too great an omission.

The hyperfine results proved difficult to interpret entirely satisfactorily. When $a \approx 1$, as appears to be supported by the $g$ factors, then $A_\parallel \approx 0$ when $k = \frac{4}{7}$. This value of $k$ leads to $A_\perp = 6\mathcal{P}/7$ which is many times too high! This is not the first time that it has proved difficult to explain Ti$^{3+}$ hyperfine structure in a crystal, for example Abraham *et al.* (1986) reported the case of tetragonally coordinated Ti$^{3+}$ in YPO$_4$ where $^{47,49}A_\parallel \approx 34\cdot9\times10^{-4}$ cm$^{-1}$ and $^{47,49}A_\perp \approx 11\cdot1\times10^{-4}$ cm$^{-1}$, but for which they were not able to explain the low values.

## 5. Conclusions

This paper reports the ESR of the only rarely observed Ti$^{3+}$ ion. At low temperatures the spectra are strong and narrow. Comparison with Ti$^{3+}$/sapphire, where the ESR spectrum cannot be seen at room temperature, and which is a very good laser material, suggests that Ti$^{3+}$/beryl, where the Ti$^{3+}$ ion is more isolated from the lattice, could be an important laser material. Preliminary optical studies have shown broad fluorescence lines and line narrowing when suitable pumping occurs (Troup *et al.* 1990). However, the crystals used had significant Cr$^{3+}$ content which may have contributed to these phenomena. Further studies are continuing with crystals of negligible Cr$^{3+}$ content.

## References

Abragam, A., and Bleaney, B. (1970). 'Electron Paramagnetic Resonance of Transition Ions' (Clarendon Press: Oxford).
Abraham, M. M., Boatner, L. A., and Ramey, J. O. (1986). *J. Chem. Phys.* **83**, 2754–8.
Bleaney, B., and O'Brien, M. C. M. (1956). *Proc. Phys. Soc. London* B **69**, 1216–30.
Deer, W. A., Howie, R. A., and Zussman, J. (1986). 'Rock Forming Minerals', 2nd edn, Vol. 1b (Longman: London).
Geusic, J. E., Peter, M., and Schulz du Bois, E. O. (1959). *Bell System Tech. J.* **38**, 291–6.
Hutton, D. R., Darmann, F. A., and Troup, G. J. (1991). *Aust. J. Phys.* **44**, 429–34.
Pilbrow, J. R. (1990). 'Transition Ion Electron Paramagnetic Resonance' (Clarendon Press: Oxford).
Stoneham, A. M. (1969). *Rev. Mod. Phys.* **41**, 82–108.
Troup, G. J., Salimbeni, R., Hutton, D. R., Pilbrow, J. R., Warne, J., McGregor, A., and Pini, R. (1990). *Quant. Electron. Plasma Phys.* **29**, 119–22.